Local spectrum analysis of field propagation in an anisotropic medium.
Part II. Time-dependent fields

Igor Tinkelman and Timor Melamed

Department of Electrical and Computer Engineering, Ben-Gurion University of the Negev, Beer Sheva 84105, Israel

In Part I of this two-part investigation [J. Opt. Soc. Am. A **22**, 1200 (2005)], we presented a theory for phase-space propagation of time-harmonic electromagnetic fields in an anisotropic medium characterized by a generic wave-number profile. In this Part II, these investigations are extended to transient fields, setting a general analytical framework for local analysis and modeling of radiation from time-dependent extended-source distributions. In this formulation the field is expressed as a superposition of pulsed-beam propagators that emanate from all space–time points in the source domain and in all directions. Using time-dependent quadratic-Lorentzian windows, we represent the field by a phase-space spectral distribution in which the propagating elements are pulsed beams, which are formulated by a transient plane-wave spectrum over the extended-source plane. By applying saddle-point asymptotics, we extract the beam phenomenology in the anisotropic environment resulting from short-pulsed processing. Finally, the general results are applied to the special case of uniaxial crystal and compared with a reference solution. © 2005 Optical Society of America

OCIS codes: 350.5500, 260.1180, 270.5530.

1. INTRODUCTION AND FORMULATION

In this paper, Part II of a two-part investigation, the theory for phase-space (PS) propagation of time-harmonic fields in an anisotropic medium with generic wave-number profile presented in Part I[1] is extended to include time-dependent fields. References to equations, figures, etc., in Part I are identified with the prefix *I* (for example, Eq. (17) in Part I is referenced to as (*I*.17)). The current study is concerned with the effects of anisotropy on the PS propagation characteristics of either an electromagnetic or a general linear time-dependent field in a lossless homogeneous medium. The time-dependent field is formulated by means of its initial distribution of either ordinary or extraordinary modes over the $z=0$ plane, denoted $u_o(\mathbf{x},t)$, by using the conventional Cartesian coordinate system $\mathbf{r}=(\mathbf{x},z)$, with $\mathbf{x}=(x_1,x_2)$. The propagation medium is characterized by a generic wave-number profile:

$$\zeta = \zeta(\boldsymbol{\xi}), \quad \boldsymbol{\xi} = (\xi_1, \xi_2). \tag{1}$$

In Eq. (1), ζ is the normalized wave number in the z-axis direction, and $\boldsymbol{\xi}$ are the normalized wave numbers in the $\mathbf{x}$ direction, all with respect to $k_o = \omega/c$, with c being a constant (more details are given Part I, Eq. (*I*.1)).

A. Time-Frequency Transforms and Analytic Signals
Given a time-dependent (TD) field $u(\mathbf{r},t)$, the corresponding frequency-domain (FD) field $\hat{u}(\mathbf{r},\omega)$ is defined by the Fourier transform relations

$$\hat{u}(\mathbf{r},\omega) = \int_{-\infty}^{\infty} \mathrm{d}t\, u(\mathbf{r},t)\exp(i\omega t), \tag{2}$$

$$u(\mathbf{r},t) = \frac{1}{2\pi}\int_{-\infty}^{\infty} \mathrm{d}\omega\,\hat{u}(\mathbf{r},\omega)\exp(-i\omega t)\mathrm{d}\omega. \tag{3}$$

As in Part I, FD fields are denoted by a caret. When necessary, we shall utilize the analytic signal formulation for time-dependent fields in order to accommodate wave constituents with evanescent spectra, as encountered in the pulsed-beam (PB) propagators. The analytic field $\overset{+}{u}(\mathbf{r},t)$ (denoted by the symbol $^+$) corresponding to the FD field $\hat{u}(\mathbf{r},\omega)$, is obtained by the one-sided Fourier inverse transform

$$\overset{+}{u}(\mathbf{r},t) = \frac{1}{\pi}\int_{0}^{\infty} \mathrm{d}\omega\,\hat{u}(\mathbf{r},\omega)\exp(-i\omega t), \quad \mathrm{Im}\, t \leq 0, \tag{4}$$

where $\hat{u}(\mathbf{r},\omega)$ is defined in Eq. (2). This integral representation can accommodate complex t with $\mathrm{Im}\,t \leq 0$; the limit for real t is related to the real signal $u(t)$ through $\overset{+}{u}(t) = u(t) + i\mathcal{H}_t u(t)$, where $\mathcal{H}_t = \mathcal{P}/\pi t \otimes$ is the Hilbert transform operator, with $\mathcal{P}$ denoting Cauchy's principal value and $\otimes$ denoting a (temporal) convolution. Thus the real field for real t is obtained through

$$u(\mathbf{r},t) = \mathrm{Re}\,\overset{+}{u}(\mathbf{r},t), \quad t \text{ real.} \tag{5}$$

B. Time-Dependent Plane-Wave Spectrum
With $u_o(\mathbf{x},t)$ representing the time-dependent field distribution over the $z=0$ plane, the analytic transient plane-wave spectrum $\overset{+}{\tilde{u}}_o(\boldsymbol{\xi},\tau)$ is defined by

$$\overset{+}{\tilde{u}}_o(\boldsymbol{\xi},\tau) = \frac{1}{\pi}\int_0^\infty d\omega \overset{+}{\hat{\tilde{u}}}_o(\boldsymbol{\xi},\omega)\exp(-i\omega\tau), \qquad (6)$$

where $\hat{\tilde{u}}_o$ is the FD plane-wave spectral distribution in Eq. (I.2). By inserting Eq. (I.2) into Eq. (6), using $k_o = \omega/c$, and inverting the order of integration (legitimate when Im $\tau \leq 0$ and in the limit of real τ), we obtain

$$\overset{+}{\tilde{u}}_o(\boldsymbol{\xi},\tau) = \int d^2x \frac{1}{\pi}\int_0^\infty d\omega \hat{u}_o(\mathbf{x},\omega)\exp[-i\omega(\tau + c^{-1}\boldsymbol{\xi}\cdot\mathbf{x})],$$

(7)

and the time-dependent spatial spectrum is found directly from the analytic data $\overset{+}{u}_o(\mathbf{x},t)$, by evaluating the inner integral in closed form, yielding

$$\overset{+}{\tilde{u}}_o(\boldsymbol{\xi},\tau) = \int d^2x \overset{+}{u}_o(\mathbf{x},\tau + c^{-1}\boldsymbol{\xi}\cdot\mathbf{x}). \qquad (8)$$

By repeating the same procedure for the plane-wave spectral representation of the anisotropic FD field in the $z > 0$ half-space in Eq. (I.4), we obtain

$$\overset{+}{u}(\mathbf{r},t) = -(2\pi c)^{-2}\int d^2\xi \partial_t^2 \overset{+}{\tilde{u}}_o\{\boldsymbol{\xi}, t - c^{-1}[\boldsymbol{\xi}\cdot\mathbf{x} + \zeta(\boldsymbol{\xi})z]\}, \quad (9)$$

and finally, the physical (real) field is given by $u(\mathbf{r},t) = \mathrm{Re}\,\overset{+}{u}(\mathbf{r},t)$.

Equation (8) is a Radon transform of $\overset{+}{u}_o(\mathbf{x},t)$ in the three-dimensional $(\mathbf{x},t)$ space, consisting of projections of $\overset{+}{u}_o(\mathbf{x},t)$ along surfaces of linear delay $t - c^{-1}\boldsymbol{\xi}\cdot\mathbf{x} = \mathrm{const}$. [see Fig. 1(a)]. It extracts from $\overset{+}{u}_o(\mathbf{x},t)$ the transient plane-wave signal that propagates in the direction of the unit vector

$$\hat{\boldsymbol{\kappa}}(\boldsymbol{\xi}) = [\boldsymbol{\xi}, \zeta(\boldsymbol{\xi})]/(\boldsymbol{\xi}\cdot\boldsymbol{\xi} + \zeta^2)^{1/2}. \qquad (10)$$

Equation (9) reconstructs the field in terms of an angular ($\boldsymbol{\xi}$) superposition of transient plane waves [see Fig. 1(b)]. The plane waves' propagation properties follow from the delay term $c^{-1}(\boldsymbol{\xi}\cdot\mathbf{x} + \zeta z)$: For $\boldsymbol{\xi}$ values such that $\zeta(\boldsymbol{\xi})$ is real, the plane waves propagate in a direction $\hat{\boldsymbol{\kappa}}(\boldsymbol{\xi})$, whereas for
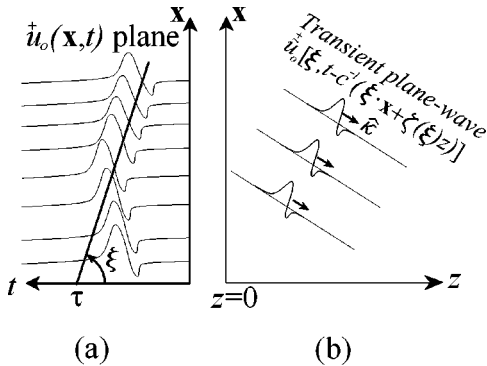
Fig. 1. Transient plane-wave spectrum. (a) The transient plane-wave distribution $\overset{+}{\tilde{u}}_o(\boldsymbol{\xi},\tau)$ is obtained by Radon transform (8) of the initial field distribution $\overset{+}{u}_o(\mathbf{x},t)$ over surfaces of linear delay $t - c^{-1}\boldsymbol{\xi}\cdot\mathbf{x} = \mathrm{const}$. (b) Transient plane-wave propagating in the direction $\hat{\boldsymbol{\kappa}}(\boldsymbol{\xi})$ of (10).

all other $\boldsymbol{\xi}$ values, where $\zeta(\boldsymbol{\xi}) = i|\zeta(\boldsymbol{\xi})|$, they decay as z increases [recall from Eq. (4) that an analytic signal decays monotonically as the imaginary part of its argument becomes more negative]. Therefore the visible spectral range, which is defined by the condition Im $\zeta(\boldsymbol{\xi}) = 0$, depends on the medium's wave-number profile $\zeta(\boldsymbol{\xi})$. For isotropic materials, where $\zeta(\boldsymbol{\xi}) = (1 - \boldsymbol{\xi}\cdot\boldsymbol{\xi})^{1/2}$, propagating plane waves occur within the $|\boldsymbol{\xi}| \leq 1$ circle in the $\boldsymbol{\xi}$ plane.

Finally, for $z = 0$, Eq. (9) is an inverse Radon transform of Eq. (8). Further details on transient plane-wave representation via real signals and short-pulse localization phenomena are given in Refs. 2–6. The plane-wave integrals in Eq. (9) are spectrally distributed. For short-pulsed signals, dominant contributions are generated by localized regions in the source domain that emphasizes radiation in a given direction. We shall not go through the asymptotic manipulations here, as our goal is not to derive analytic ray-type local approximations. Instead, in Subsection 1.C we shall show how phase-space processing yields spectral representations that are *a priori* localized about ray trajectories.

C. Phase-Space Processing in the Time Domain

The TD local spectrum of the data is defined as the inverse Fourier transform [Eq. (3)] of the FD PS distribution $\hat{U}_o(\bar{\mathbf{X}})$ in Eq. (I.8),

$$U_o(\bar{\mathbf{Y}}) = \frac{1}{2\pi}\int d\omega \hat{U}_o(\bar{\mathbf{X}},\omega)\exp(-i\omega\bar{t}), \qquad (11)$$

where $\bar{t}$ denotes the phase-space time variable in the five-dimensional PS domain $\bar{\mathbf{Y}} \equiv (\bar{\mathbf{x}}, \bar{\boldsymbol{\xi}}, \bar{t})$. To deduce $U_o(\bar{\mathbf{Y}})$ directly from the TD field distribution, we insert Eq. (I.8) into Eq. (11) and interchange the orders of integration to obtain

$$U_o(\bar{\mathbf{Y}}) = \int d^2x \int dt u_o(\mathbf{x},t) W(\mathbf{x},t;\bar{\mathbf{Y}}), \qquad (12)$$

where the space–time-dependent kernel function W is given by

$$W(\mathbf{x},t;\bar{\mathbf{Y}}) = w[\mathbf{x} - \bar{\mathbf{x}}, t - \bar{t} - c^{-1}\bar{\boldsymbol{\xi}}\cdot(\mathbf{x} - \bar{\mathbf{x}})] \qquad (13)$$

and the TD window $w(\mathbf{x},t)$ is the time-domain analog of $\hat{w}(\mathbf{x})$ in Eq. (I.8), obtained with Eq. (3). The space–time and spectral dependence of the phase-space window in Eq. (13) implies that the PS kernel W is localized about $(\bar{\mathbf{x}}, \bar{t})$ with spectral tilt $\bar{\boldsymbol{\xi}}$, as schematized in Fig. 2. The operation in Eq. (12), is termed local Radon transform, which extracts the local spectral information from the TD distribution $u_o(\mathbf{x},t)$.

In the present context of anisotropic propagation, where $u_o(\mathbf{x},t)$ is either an ordinary- or an extraordinary-mode distribution, it is convenient to describe the local spectrum by the initial TD plane-wave distribution, $\tilde{u}_o(\boldsymbol{\xi},\tau)$, which is obtained by matching to the source TD plane-wave representation. By inserting Eqs. (I.9) into Eq. (11) and inverting the order of integration, we obtain
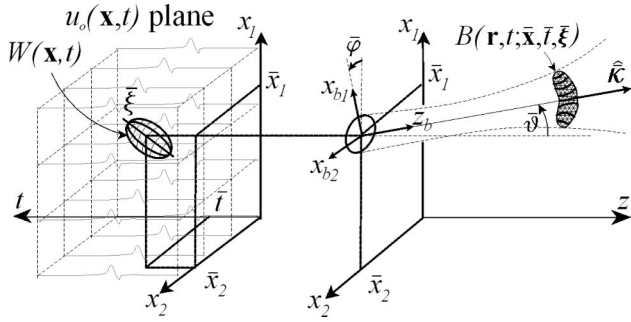
Fig. 2.   Local (phase-space) spectrum and local beam coordinates. The PS spectral distribution is obtained by windowing of $u_o(\mathbf{x},t)$ in the three-dimensional $(\mathbf{x},t)$ domain with a time-dependent window $w(\mathbf{x},t)$, which is shifted to the space–time point $(\bar{\mathbf{x}},\bar{t})$ and is tilted by a linear delay of $\bar{\boldsymbol{\xi}}\cdot(\mathbf{x}-\bar{\mathbf{x}})$. Thus the PS transform extracts local directional properties of $u_o(\mathbf{x},t)$ and by that matches a single PB propagator emanating from the window center at $(\bar{\mathbf{x}},\bar{t})$ along $\hat{\bar{\boldsymbol{\kappa}}}$.

$$U_o(\bar{\mathbf{Y}}) = -(2\pi c)^{-2}\int d^2\xi \int d\tau \tilde{u}_o(\boldsymbol{\xi},\tau)\partial_\tau^2\tilde{w}(\boldsymbol{\xi}-\bar{\boldsymbol{\xi}},\tau-\bar{t}$$
$$+ c^{-1}\boldsymbol{\xi}\cdot\bar{\mathbf{x}}), \tag{14}$$

where $\tilde{w}(\boldsymbol{\xi},\tau)$ denotes the transient plane-wave spectrum [Eq. (8)] of $w(\mathbf{x},t)$.

To synthesize the field distribution $u_o(\mathbf{x},t)$ from PS distribution (12), we apply Eq. (3) to Eq. (I.10) and follow essentially the same analytic steps as in Eqs. (11)–(13), obtaining

$$u(\mathbf{x},t) = -(2\pi c)^{-2}\int d^5\bar{Y}U(\bar{\mathbf{Y}})W_N(\mathbf{x},t;\bar{\mathbf{Y}}), \tag{15}$$

where

$$W_N(\mathbf{x},t;\bar{\mathbf{Y}}) = N^{-1}(t) \overset{t}{\otimes} W(\mathbf{x},t;\bar{\mathbf{Y}}), \tag{16}$$

with $\overset{t}{\otimes}$ denoting a (temporal) convolution and

$$N^{-1}(t) = \frac{1}{2\pi}\int d\omega(-i\omega)^2\hat{N}^{-2}(\omega)\exp(-i\omega t), \tag{17}$$

where the $\mathcal{L}_{\mathbf{x}}^2$ norm of $\hat{w}$, $\hat{N}(\omega)$, is defined in Eq. (I.11). Using Eq. (I.11) in Eq. (17), we note that $N^{-1}(t)\otimes$ is the inverse operator associated with $N(t)\otimes$, where

$$N(t) = \partial_t^{-2}\int d^2x\, w(\mathbf{x},t) \otimes w(\mathbf{x},-t), \tag{18}$$

with ∂_t^{-2} denoting a double (temporal) integration. Any formal convergence problems of N^{-1} that may arise as $\omega \rightarrow \infty$ are avoided for practical finite-bandwidth signals with upper frequency limits, for which the integral limits in Eq. (17) may be restricted to the signal $u_o(\mathbf{x},t)$ frequency content.

The windowed integral representation in Eq. (15) synthesizes the space–time initial distribution as a phase-space superposition of *all* local spectral contributions $\bar{\boldsymbol{\xi}}$ from *all* space–time points $(\bar{\mathbf{x}},\bar{t})$. Recalling the discussion following Eq. (I.8), the windowed spectrum at a point $\bar{\mathbf{x}}$ is typically concentrated around a time $\bar{t}(\bar{\mathbf{x}})$ and wave num-

ber (or wave tilt) $\bar{\boldsymbol{\xi}}(\bar{\mathbf{x}})$ that describe the arrival time and direction of the field that is propagating toward the $z=0$ plane at that point. Inverse transform Eq. (15) at $(\mathbf{x},t)$ is therefore localized *a priori* about the phase-space subdomain $\bar{\mathbf{Y}}(\bar{\mathbf{x}})=[\bar{\mathbf{x}},\bar{\boldsymbol{\xi}}(\bar{\mathbf{x}}),\bar{t}(\bar{\mathbf{x}})]$.

In the time domain, each window kernel $W_N(\mathbf{x},t;\bar{\mathbf{Y}})$ in Eq. (15) gives rise to a propagating PB field $B(\mathbf{r},t;\bar{\mathbf{Y}})$ in the $(\mathbf{r},t)$ configuration space, whose axis emerges from $\bar{\mathbf{x}}$ on the initial $z=0$ plane in a $\bar{\boldsymbol{\xi}}$-dependent direction. Therefore Eq. (15) can be propagated into $z>0$, giving

$$u(\mathbf{r},t) = -(2\pi c)^{-2}\int d^5\bar{Y}U_o(\bar{\mathbf{Y}})B(\mathbf{r},t;\bar{\mathbf{Y}}), \tag{19}$$

where the anisotropic propagators $B(\mathbf{r},t;\bar{\mathbf{Y}})$ describe the radiation into the half-space $z>0$ that is due to the initial distribution $W_N(\mathbf{x},t;\bar{\mathbf{Y}})$ over the $z=0$ plane (see Fig. 2).

In the present context of anisotropic propagation, it is convenient to express the PB propagators by a TD plane-wave representation, which is easily obtained by using the generic wave-number profile $\zeta(\boldsymbol{\xi})$ in Eq. (1) [compare with Eq. (I.13)]. Since B contains an evanescent spectrum in addition to the propagating one, we shall utilize analytic signal representation (9). Thus $B(\mathbf{r},t;\bar{\mathbf{Y}})$ $=\mathrm{Re}\,\overset{+}{B}(\mathbf{r},t;\bar{\mathbf{Y}})$ with

$$\overset{+}{B}(\mathbf{r},t;\bar{\mathbf{Y}}) = -(2\pi c)^{-2}\int d^2\xi\partial_t^2\overset{+}{\tilde{W}}_N[\boldsymbol{\xi},t-c^{-1}(\boldsymbol{\xi}\cdot\mathbf{x}+\zeta(\boldsymbol{\xi})z);\bar{\mathbf{Y}}], \tag{20}$$

where $\overset{+}{\tilde{W}}_N(\boldsymbol{\xi},\tau;\bar{\mathbf{Y}})$ is the analytic transient plane-wave spectrum [Eq. (8)] of $W_N(\mathbf{x},t;\bar{\mathbf{Y}})$, which may be evaluated either from the FD plane-wave spectral window $\hat{\tilde{w}}(\boldsymbol{\xi})$ in Eqs. (I.9),

$$\overset{+}{\tilde{W}}_N(\boldsymbol{\xi},\tau;\bar{\mathbf{Y}}) = \frac{1}{\pi}\int_0^\infty d\omega[-i\omega/\hat{N}(\omega)]^2$$
$$\times\hat{\tilde{W}}(\boldsymbol{\xi};\bar{\mathbf{X}},\omega)\exp[-i\omega(\tau-\bar{t})], \tag{21}$$

or directly from the TD spectral window $\overset{+}{\tilde{w}}(\boldsymbol{\xi},\tau)$,

$$\overset{+}{\tilde{W}}_N(\boldsymbol{\xi},\tau;\bar{\mathbf{Y}}) = N^{-1}(t) \otimes \overset{+}{\tilde{w}}(\boldsymbol{\xi}-\bar{\boldsymbol{\xi}},\tau-\bar{t}+c^{-1}\boldsymbol{\xi}\cdot\bar{\mathbf{x}}), \tag{22}$$

where $\overset{+}{\tilde{w}}(\boldsymbol{\xi},\tau)$ denotes the analytic plane-wave spectrum [Eq. (8)] of $\overset{+}{\tilde{w}}(\mathbf{x},t)$, and $N^{-1}(t)$ is given in Eq. (17). Alternatively, the TD PS propagator $\overset{+}{B}$ may be obtained from the FD PS propagator $\hat{B}$ by

$$\overset{+}{B}(\mathbf{r},t;\bar{\mathbf{Y}}) = \frac{1}{\pi}\int_0^\infty d\omega[-i\omega/\hat{N}(\omega)]^2\hat{B}(\mathbf{r};\mathbf{X},\omega)\exp[-i\omega(t-\bar{t})]. \tag{23}$$

D. Quadratic-Lorentzian Windows

A convenient TD window is obtained by transforming the FD Gaussian window Eqs. (I.14), with Γ being frequency independent. Note, though, that convergence of the window in Eqs. (I.14) implies $\Gamma|_{\omega<0} = -\Gamma^*|_{\omega>0}$, so it is convenient to utilize the analytic signal representation [Eq. (4)]. Furthermore, in order to obtain a TD window in $\mathcal{L}^1_{(\mathbf{x},t)}$ (i.e., $\int |w(\mathbf{x},t)| \mathrm{d}^2 x \, \mathrm{d}t < \infty$) as required for numerical implementation of Eq. (12), it is desirable to multiply the FD Gaussian window in Eqs. (I.14) by a frequency dependence of $(-i\omega)^2 \exp(-\frac{1}{2}\omega T)$, where the parameter $T>0$ is chosen to satisfy

$$T \ll \omega_{\max}^{-1}, \tag{24}$$

with $\omega_{\max}$ denoting the upper frequency of $u_o(\mathbf{x},t)$. Thus the time-harmonic Gaussian windows are given by

$$\hat{w}(\mathbf{x}) = (-i\omega)^2 \exp\left(-\frac{1}{2}\omega T + \frac{1}{2}k_o \mathbf{x}\Gamma\mathbf{x}^T\right), \tag{25}$$

and the $\mathcal{L}^2_{\mathbf{x}}$ norm of these windows is obtained by inserting Eq. (25) into Eq. (I.11), giving

$$\hat{N}^2(\omega) = c\pi\omega^3 \exp(-\omega T)/\Gamma_i. \tag{26}$$

Note that $\hat{N}^{-2}(\omega)$ grows exponentially with ω and therefore the integral in Eq. (17), which defines the corresponding TD operator $N^{-1}\otimes$, does not converge. Nevertheless, we assume that $u_o(\mathbf{x},t)$ has an upper frequency (as any physical or sampled signal) and that T is chosen according to condition (24). Thus we may use $\exp(-\omega T) \approx 1$ over $w \leq w_{\max}$ in Eq. (26), yielding

$$\hat{N}^2(\omega) = c\pi\omega^3/\Gamma_i, \quad \omega \leq \omega_{\max}. \tag{27}$$

The quadratic-Lorentzian windows are obtained by inserting Eq. (25) into Eq. (4), giving

$$w(\mathbf{x},t) = \mathrm{Re}\, \overset{+}{w}(\mathbf{x}) = \mathrm{Re}\, \overset{+}{\delta}''\left(t - \frac{i}{2}T - c^{-1}\frac{1}{2}\mathbf{x}\Gamma\mathbf{x}^T\right), \tag{28}$$

where $\overset{+}{\delta}$ is the analytic delta function $\overset{+}{\delta}(t) = (\pi i t)^{-1}$ for $\mathrm{Im}\,t < 0$, so that $\overset{+}{\delta}''(t) = 2/\pi i t^3$. This TD window is localized around $(\mathbf{x},t) = (0,0)$; for $|\mathbf{x}| = 0$, it peaks at $t = 0$ and decays thereafter as t^{-3}. For $|\mathbf{x}| \neq 0$, the argument of the $\overset{+}{\delta}$ function in Eq. (28) has a negative imaginary part, and thus the window has the form of a (double-differentiated) smooth Lorentzian pulse.

2. ORDINARY PULSED-BEAM PROPAGATORS

In this section we shall briefly derive the expressions for the PB propagators for the *ordinary* field distribution, for which, for a proper choice of the constant c, the wavenumber profile is given by

$$\zeta(\boldsymbol{\xi}) = (1 - \xi^2)^{1/2}, \quad \xi^2 \equiv \boldsymbol{\xi}\cdot\boldsymbol{\xi}, \quad \mathrm{Im}\,\zeta \geq 0. \tag{29}$$

A. Pulsed-Beam Propagators
The PB propagators corresponding to the quadratic-Lorentzian windows in Eq. (28) are given by the formal

transient plane-wave integral Eq. (20). Alternatively, they may be evaluated by multiplying the FD beam propagator $\hat{B}$ in Eq. (I.19) by $(-i\omega)^2 \exp(-\frac{1}{2}\omega T)$ and inserting with Eq. (27) into analytic Fourier inversion (23), giving

$$\overset{+}{B}(\mathbf{r},t;\overline{\mathbf{Y}}) = \left[\frac{\det\Gamma(z_b)}{\det\Gamma(0)}\right]^{1/2} \frac{i\Gamma_i}{\pi c}\frac{1}{\pi}\int_0^\infty \mathrm{d}\omega(-i\omega)$$
$$\times \exp\left\{-i\omega\left[t - \overline{t} - \frac{i}{2}T - c^{-1}S(\mathbf{r})\right]\right\}, \tag{30}$$

$$S(\mathbf{r}_b) = z_b + \frac{1}{2}\mathbf{x}_b\Gamma(z_b)\mathbf{x}_b^T. \tag{31}$$

Evaluating the $\mathrm{d}\omega$ integration in closed form, we obtain

$$\overset{+}{B}(\mathbf{r},t;\overline{\mathbf{Y}}) = \frac{i\Gamma_i}{\pi c}\left[\frac{\det\Gamma(z_b)}{\det\Gamma(0)}\right]^{1/2}\overset{+}{\delta}'[t - \overline{t} - \tau(\mathbf{r}_b)], \tag{32}$$

where

$$\tau(\mathbf{r}_b) = -\frac{i}{2}T + c^{-1}S(\mathbf{r}_b) \tag{33}$$

and $\overset{+}{\delta}'(t) = -1/(\pi i t^2)$. PB field (32) is written in terms of the beam coordinates (x_{b_1}, x_{b_2}, z_b) defined in Eq. (I.18), and Γ is given in Eq. (I.20). This expression readily establishes $\overset{+}{B}(\mathbf{r},t;\overline{\mathbf{Y}})$ as a PB field that emanates from the space–time point $(\mathbf{x},t) = (\overline{\mathbf{x}},\overline{t})$ in the $z = 0$ plane, and it propagates in the $\hat{\overline{\boldsymbol{\kappa}}}_{\mathrm{iso}} = [(\overline{\boldsymbol{\xi}}, (1-\overline{\xi}^2))]^{1/2}$ direction along the z_b axis.

The PB field may now be characterized by rewriting the elements of $\Gamma(z_b) = \mathrm{diag}[\Gamma_1(z_b), \Gamma_2(z_b)]$ in the form

$$\Gamma_{1,2}(z_b) = 1/R_{1,2}(z_b) + i/I_{1,2}(z_b), \tag{34}$$

with

$$R_{1,2} = (z_b - Z_{1,2}) + F_{1,2}^2/(z_b - Z_{1,2}), \tag{35}$$

$$I_{1,2}(z_b) = F_{1,2}[1 + (z_b - Z_{1,2})^2/F_{1,2}^2], \tag{36}$$

where $Z_{1,2}$ and $F_{1,2}$ are given in Eqs. (I.21) and (I.22), respectively.

The complex delay, $\tau(\mathbf{r}_b)$, in Eq. (33) may now be written in a standard form,

$$\tau(\mathbf{r}_b) = t_p(\mathbf{r}_b) + (i/2)T_p(\mathbf{r}_b), \tag{37}$$

where we define

$$t_p(\mathbf{r}_b) = c^{-1}[z_b + x_{b_1}^2/(2R_1) + x_{b_2}^2/(2R_2)], \tag{38}$$

$$T_p(\mathbf{r}_b) = T + c^{-1}(x_{b_1}^2/I_1 + x_{b_2}^2/I_2). \tag{39}$$

Expression (32) with Eqs. (37)–(39) is readily identified as an astigmatic PB whose major axes are x_{b_1} and x_{b_2}. Clearly, from Eq. (37), $t_p(\mathbf{r})$ is the paraxial propagation delay along the z_b axis, and hence $R_{1,2}$ are the wave-front radii of curvature in the $x_{b_{1,2}}$ directions.

For a given observation point $\mathbf{r}_b$, the beam field peaks at $t - \overline{t} = t_p(\mathbf{r}_b)$, and its half-amplitude pulse length and peak value are given, respectively, by $T_p(\mathbf{r}_b)(\sqrt{5}-2)^{1/2}$ and $4/\pi T_p^2(\mathbf{r}_b)$. The transverse half-amplitude diameters of

the PB propagator in the $(x_{b_{1,2}}, z_b)$ cross-sectional planes $D_{1,2}$ may be obtained by solving $T_p(\mathbf{r}_b) = \sqrt{2} T_p(0)$, giving

$$D_{1,2}(z_b) = 2[(\sqrt{2}-1)cTI_{1,2}(z_b)]^{1/2}. \quad (40)$$

The collimation lengths in the $(x_{b_{1,2}}, z_b)$ cross-sectional planes are $F_{1,2}$, and the waists are located at $z_b = Z_{1,2}$ with the corresponding widths $2[cTF_{1,2}(\sqrt{2}-1)]^{1/2}$. From Eq. (40) with Eq. (36), we note that in the collimation (Fresnel) zone $|z_b - Z_{1,2}| < F_{1,2}$, the PB is essentially unaffected by the propagation, whereas outside this zone, B opens up along a far-field diffraction angle $\Theta_{1,2} = 2[(\sqrt{2}-1)cT/F_{1,2}]^{1/2}$.

B. Phase-Space Localization in the Time Domain

As discussed in connection with Eq. (15), the TD phase-space representation is localized *a priori* around the coordinates $\overline{\mathbf{Y}} = [\overline{\mathbf{x}}, \overline{\boldsymbol{\xi}}(\overline{\mathbf{x}}), \overline{t}(\overline{\mathbf{x}})]$ since the local spectrum of the data $U_o(Y)$ is concentrated there. Further localization is effected by the PB propagators $B(\mathbf{r}, t; \overline{\mathbf{Y}})$, which are concentrated around the trajectories $\hat{\overline{\boldsymbol{\kappa}}}_{\text{iso}}$. This constrains the PS integration domain to the vicinity of the observation manifold $\overline{\mathbf{Y}}(\mathbf{r}, t)$, whose $(\overline{\mathbf{x}}, \overline{\boldsymbol{\xi}}, \overline{t})$ coordinates are defined by

$$(\mathbf{x} - \overline{\mathbf{x}})/\overline{R} = \overline{\boldsymbol{\xi}}, \quad \overline{t} = t - c^{-1}\overline{R}, \quad (41)$$

where $\overline{R} = (|\mathbf{x} - \overline{\mathbf{x}}|^2 + z^2)^{1/2}$.

3. EXTRAORDINARY PULSED-BEAM PROPAGATORS

A. Asymptotic Evaluation and Parameterization

The extraordinary PB propagators $\overset{+}{B}(\mathbf{r}, t; \overline{\mathbf{Y}})$ for the generic anisotropic wave-number profile $\zeta(\boldsymbol{\xi})$ may be obtained from the frequency-domain asymptotic propagator $\hat{B}(\mathbf{r}, \overline{\mathbf{X}})$. By multiplying the FD anisotropic beam in Eq. (I.40) by $(-i\omega)^2 \exp(-\frac{1}{2}\omega T)$, we obtain the FD propagator corresponding to the FD Gaussian window in Eq. (25),

$$\hat{B}(\mathbf{r}; \overline{\mathbf{X}}) = (-i\omega)^2 \left[\frac{\det \boldsymbol{\Gamma}(z_b)}{\det \boldsymbol{\Gamma}(0)} \right]^{1/2}$$

$$\times \exp \left\{ -i\omega \left[\frac{i}{2}\omega T - c^{-1}S(\mathbf{r}_b) \right] \right\}, \quad (42)$$

$$S(\mathbf{r}_b) = \hat{\overline{\boldsymbol{\kappa}}}_{\text{iso}} \cdot [\mathbf{r} - (\overline{\mathbf{x}}, 0)] + \tfrac{1}{2}\mathbf{x}_b \boldsymbol{\Gamma}(z_b)\mathbf{x}_b^T, \quad (43)$$

where $\hat{\overline{\boldsymbol{\kappa}}}_{\text{iso}} = (\overline{\boldsymbol{\xi}}, \overline{\zeta})$, and the analytic PB propagator may be obtained by inserting Eq. (43) with Eq. (27) into Eq. (23), giving

$$\overset{+}{B}(\mathbf{r}, t; \overline{\mathbf{Y}}) = \frac{1}{\pi} \int_0^\infty d\omega \frac{\omega \Gamma_i}{c\pi} \left[\frac{\det \boldsymbol{\Gamma}(z_b)}{\det \boldsymbol{\Gamma}(0)} \right]^{1/2}$$

$$\times \exp \left\{ -i\omega \left[t - \overline{t} + \frac{i}{2}\omega T - c^{-1}S(\mathbf{r}_b) \right] \right\}. \quad (44)$$

Integral (44) may be evaluated in closed form, giving

$$B(\mathbf{r}, t; \overline{\mathbf{Y}}) = \text{Re} \frac{i\Gamma_i}{\pi c} \left[\frac{\det \boldsymbol{\Gamma}(z_b)}{\det \boldsymbol{\Gamma}(0)} \right]^{1/2} \overset{+}{\delta}'[t - \overline{t} - \tau(\mathbf{r}_b)], \quad (45)$$

where

$$\tau(\mathbf{r}_b) = -\frac{i}{2}T + c^{-1}S(\mathbf{r}_b) \quad (46)$$

and $\overset{+}{\delta}'(t) = -1/(\pi i t^2)$. Asymptotic expression (45) is identified as an astigmatic pulsed beam propagating in the direction of $\hat{\overline{\boldsymbol{\kappa}}}(\overline{\boldsymbol{\xi}})$ in Eq. (I.30) (see Fig. 2).

To clarify the properties of the anisotropic PB propagator in Eq. (45), we rewrite the arguments of the $\overset{+}{\delta}$ function in a standard form,

$$\text{Re } i\overset{+}{\delta}' \left[t - \overline{t} - t_p - \frac{i}{2}T_p \right] = \frac{-1}{\pi} \frac{(t - \overline{t} - t_p)^2 - (T_p/2)^2}{[(t - \overline{t} - t_p)^2 + (T_p/2)^2]^2}, \quad (47)$$

where we define

$$t_p(\mathbf{r}) = c^{-1}(\hat{\overline{\boldsymbol{\kappa}}}_{\text{iso}} \cdot \mathbf{r} + x_{b_1}^2/2R_1 + x_{b_2}^2/2R_2), \quad (48)$$

$$T_p(\mathbf{r}) = T + c^{-1}(x_{b_1}^2/I_1 + x_{b_2}^2/I_2), \quad (49)$$

where

$$I_{1,2}(z_b) = a_{1,2}F_{1,2}[1 + (z_b - Z_{1,2})^2/F_{1,2}^2], \quad (50)$$

and $R_{1,2}$ is given in Eq. (I.49), with $Z_{1,2}$ and $F_{1,2}$ in Eq. (I.46). The isotropy-dependent parameters $a_{1,2}$ and their relation to the wave-number surface normal and curvatures have been discussed with connection with Eq. (I.45).

In a manner similar to that for the parameterization of the isotropic beam field in Eq. (32), one identifies Eq. (45) with Eqs. (48) and (49) as an astigmatic PB whose major axes are x_{b_1} and x_{b_2}, where $t_p(\mathbf{r}_b)$ is the paraxial propagation delay along the beam axis and $R_{1,2}$ are the wave-front radii of curvature in the $x_{b_{1,2}}$ directions. For a given observation point $\mathbf{r}_b$, the beam field peaks at $t - \overline{t} = t_p(\mathbf{r}_b)$, and its half-amplitude pulse length and peak value are given, respectively, by $T_p(\mathbf{r}_b)(\sqrt{5}-2)^{1/2}$ and $4/\pi T_p^2(\mathbf{r}_b)$. The PB transverse half-amplitude diameters in the $\mathbf{x}_{b_1}$ directions, $D_{1,2}$, may be obtained by solving $T_p(\mathbf{r}_b) = \sqrt{2}T_p(0)$, giving

$$D_{1,2}(z_b) = 2[(\sqrt{2}-1)cTI_{1,2}(z_b)]^{1/2}, \quad (51)$$

where $I_{1,2}$ are given in Eq. (50). The collimation lengths in the $(x_{b_{1,2}}, z)$ cross-sectional planes are $F_{1,2}$, and the waists are located at $z_b = Z_{1,2}$ with the corresponding widths $2[cTa_{1,2}F_{1,2}(\sqrt{2}-1)]^{1/2}$. From Eq. (51) with Eq. (50), one notes that in the collimation (Fresnel) zone $|z_b - Z_{1,2}| < F_{1,2}$, the PB is essentially unaffected by the propagation, whereas outside this zone, B opens up along a far-field diffraction angle $\Theta_{1,2} = 2[(\sqrt{2}-1)cTa_{1,2}/F_{1,2}]^{1/2}$. Recalling the discussion following Eq. (I.49), the representation in Eqs. (49)–(51) parameterizes the PB propagators in terms of local geometrical properties (normal and curvatures) of the generic wave-number surface $\zeta(\boldsymbol{\xi})$ about the PS directional processing parameter $\boldsymbol{\xi} = \overline{\boldsymbol{\xi}}$

(see Fig. *I*.2).

B. Phase-Space Localization in the Time Domain
In addition to *a priori* localization of the PS spectral distribution that was discussed in connection with Eq. (15), further localization is effected by the extraordinary PB propagators $B(\mathbf{r},t;\bar{\mathbf{Y}})$, which are concentrated around the trajectories $\hat{\bar{\boldsymbol{\kappa}}}$ in Eq. (*I*.30). This constrains the phase-space integration domain to the vicinity of the medium-dependent extraordinary observation manifold $\bar{\mathbf{Y}}(\mathbf{r},t)$, whose $(\bar{\mathbf{x}},\bar{\boldsymbol{\xi}},\bar{t})$ coordinates are defined by

$$(\mathbf{x}-\bar{\mathbf{x}})/\bar{R} = \cos\bar{\vartheta}_{1,2}, \quad \bar{t} = t - c^{-1}[|\mathbf{x}-\bar{\mathbf{x}}|^2 + (z)^2]^{1/2}, \quad (52)$$

with $\bar{\vartheta}_{1,2}$ being the beam-axis angles with respect to the (x_1,x_2) axes, respectively [see Eq. (*I*.30) and Fig. *I*.2]. Note that this constraint matches observation angles $(\mathbf{x}-\bar{\mathbf{x}})/\bar{R}$ to the normal of the wave-number surface at the PS (directional) parameter $\boldsymbol{\xi}=\bar{\boldsymbol{\xi}}$.

4. ILLUSTRATIVE EXAMPLE

A. Reference Solution
The TD PB propagators corresponding to quadratic-Lorentzian windows (28) were evaluated asymptotically in the short-pulsed processing regime and parameterized in Section 3. To illustrate these expressions, we compare them with a reference solution, which is generated by using the transient plane-wave exact formulation [Eq. (20)].

The transient plane-wave distribution $\overset{+}{\tilde{W}}(\boldsymbol{\xi},\tau)$ corresponding to the quadratic-Lorentzian windows in Eq. (28) is obtained by (a) multiplying $\hat{\tilde{w}}$ in Eq. (*I*.14) by $(-i\omega)^2 \times\exp(-\frac{1}{2}\omega T)$ and inserting into Eq. (*I*.9) to obtain the corresponding FD plane-wave distribution,

$$\hat{\tilde{W}}(\boldsymbol{\xi};\bar{\mathbf{X}}) = \frac{-i\omega 2\pi c}{\Gamma}\exp\left(-i\omega\left\{\frac{-iT}{2}\right.\right.$$
$$\left.\left.+ c^{-1}\left[\frac{1}{2}(\boldsymbol{\xi}-\bar{\boldsymbol{\xi}})\Gamma^{-1}(\boldsymbol{\xi}-\bar{\boldsymbol{\xi}})^T + \boldsymbol{\xi}\cdot\bar{\mathbf{x}}\right]\right\}\right), \quad (53)$$

and (b) inserting Eq. (53) with Eq. (27) into Eq. (21). The resulting Fourier transform may be evaluated in closed form, giving

$$\overset{+}{\tilde{W}}_N(\boldsymbol{\xi},\tau;\bar{\mathbf{Y}}) = \frac{2i\Gamma_i}{\Gamma}\overset{+}{\delta}\left\{\tau-\bar{t}+\frac{-iT}{2}\right.$$
$$\left.+ c^{-1}\left[\frac{1}{2}(\boldsymbol{\xi}-\bar{\boldsymbol{\xi}})\Gamma^{-1}(\boldsymbol{\xi}-\bar{\boldsymbol{\xi}})^T + \boldsymbol{\xi}\cdot\bar{\mathbf{x}}\right]\right\}. \quad (54)$$

The field representation in Eq. (20) with Eq. (54) is an exact formulation and therefore may be regarded as a reference solution for $\overset{+}{B}(\mathbf{r},t)$. In Subsection 4.B we shall compare this reference solution with the asymptotic PB field for the special case of the uniaxial extraordinary wave-number profile in Eq. (*I*.54), namely,

$$\zeta(\boldsymbol{\xi}) = [1 - (\xi_2^2 + \xi_1^2)/\epsilon_z]^{1/2}, \quad c = c_0/\sqrt{\epsilon}. \quad (55)$$

All simulations are carried out for beam parameters $\Gamma_{1,2}=-1+i$, $cT=0.001$, $\bar{\xi}_1=0.3$, $\bar{\xi}_2=0.5$, and for medium parameters $\epsilon=1$, $\epsilon_z=1.3$.
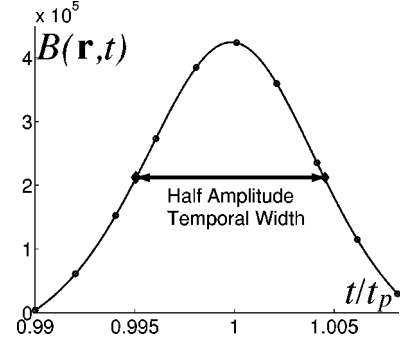
Fig. 3. PB on-axis temporal distribution. The solid curve plots the asymptotic on-axis field for $z_b=0.005$ as a function of time, and circles plot the reference solution.

(a)

(b)

(c)
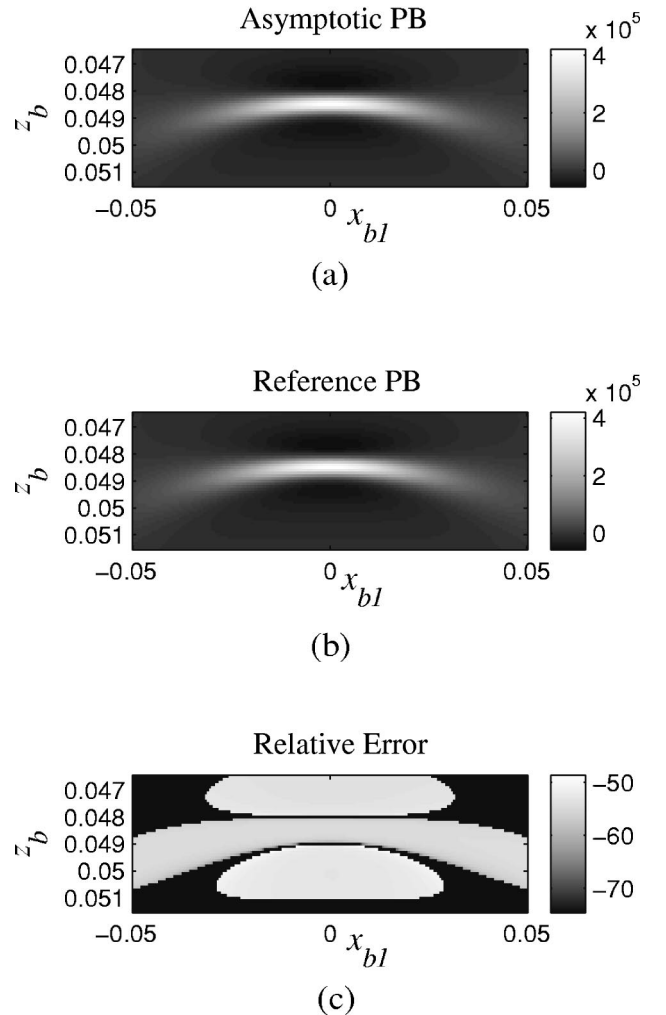
Fig. 4. Snapshots of (a) the asymptotic and (b) the reference field in the (x_{b_1},z_b) plane. (c) Relative error in decibels for points where the reference field is more than -30 db from its on-axis peak.
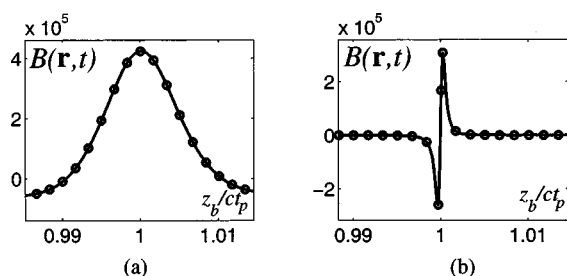
Fig. 5. Snapshots of PB propagator on-axis PB distributions as a function of z_b for (a) the near ($t=0.05$) and (b) the far ($t=1$) field. The solid curves depict the asymptotic propagator, and circles represent the reference solution.
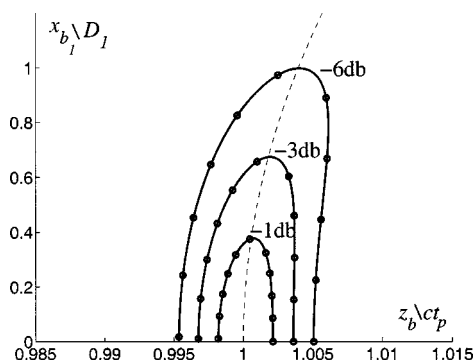
Fig. 6. Contour plots of -1, -3, and -6 db from peak level of the off-axis PB-propagator distribution in the (x_{b_1}, z_b) cross-sectional plane, for both the asymptotic (solid curves) and the reference field (circles). The dashed curve represents the radius of curvature.

B. Pulsed-Beam On-Axis Temporal Distribution

The on-axis ($\mathbf{x}_b=0$) field in $z_b=0.005$ as a function of time is presented in Fig. 3. The asymptotic field in Eq. (45) is plotted as a solid curve, and the reference solution is plotted with circles. The time axis is normalized with respect to the on-axis propagation delay $t_p|_{\mathbf{x}_b=0}$ in Eq. (48) so that the pulsed beam is centered at $t/t_p=1$. The half-amplitude temporal width $T(\sqrt{5}-2)^{1/2}$ is plotted at the half-on-axis peak of $4/\pi T^2$ [see the parameterization following Eq. (49)]. Clearly, the asymptotic solution as well as the parameterization agrees very well with the TD plane-wave reference solution.

C. Asymptotic and Reference-Field Comparison

Snapshots at $t=0.05$ of the asymptotic [Eq. (32)] and the reference [Eq. (54)] fields over the (x_{b_1}, z_b) cross-sectional plane are presented in Figs. 4(a) and 4(b), respectively. The relative error in decibels, $|B_{\text{asymp}}-B_{\text{ref}}|/|B_{\text{ref}}|$, is depicted in Fig. 4(c) for points where the reference field is over -30 db from its on-axis peak, for which the relative error is found to be less than -48 db, demonstrating the good agreement between the two.

D. On-Axis Field Distribution

Snapshots of PB propagator on-axis distributions as a function of z_b, for near ($t=0.05$ s) and far ($t=1$ s) fields are presented in Figs. 5(a) and 5(b), respectively. Asymptotic propagator (32) is depicted by solid curves, and reference solution (54) is represented by circles to demonstrate the

accuracy of the asymptotics for both near and far fields. The figure also demonstrates the temporal changes of the Lorentzian pulse as it goes to a Hilbert transformation from near- to far-field distributions. For clarity, the z_b axis was normalized by ct_p so that the beam center is at $z_b/ct_p=1$ for both cases.

E. Off-Axis Distribution and Parameterization

Contour plots of -1, -3 and -6 db from peak level of the off-axis PB-propagator distribution in the (x_{b_1}, z_b) cross-sectional plane are presented in Fig. 6 for both the asymptotic field (solid curves) and the reference field (circles). The x_{b_1} axis is normalized by the PB half-amplitude diameter D_1, so that the -6 db curve is bounded by $x_{b_1}/D_1=1$, as can be seen in the figure. The z_b (horizontal) axis is normalized by the propagation distance of the beam center ct_p, so that the center is at $z/ct_p=1$, from which a circle of radius R_1 [the wave-front radius of curvature in Eq. (I.49)] is plotted with a dashed curve.

5. CONCLUSION

In this paper, Part II of a two-part investigation, we have presented a theory for phase-space propagation of TD fields in an anisotropic medium characterized by a generic wave-number profile. Using TD quadratic-Lorentzian windows for the local processing of either ordinary or extraordinary field distributions, we represented the field by a PS spectral distribution in which the propagating elements are pulsed beams. By applying saddle-point asymptotics, we extracted the beam phenomenology in the anisotropic environment resulting from short-pulsed processing. The PB-propagator parameters were mapped to local geometrical properties of the generic wave-number profile. Finally, the general results were applied to the special case of uniaxial crystal and were compared with a TD reference solution and found to agree remarkably well. The present investigation may be extended to propagation in an inhomogeneous medium, in which each of the PB windows is propagated through the anisotropic inhomogeneous medium in a manner similar to that for propagation in an inhomogeneous isotropic medium presented in Ref. 7.

REFERENCES

1. I. Tinkelman and T. Melamed, "Local spectrum analysis of field propagation in anisotropic media. Part I. Time-harmonic fields," J. Opt. Soc. Am. A, **22**, 1200–1207 (2005).
2. E. Heyman and L. B. Felsen, "Weakly dispersive spectral theory of transients (STT), part I: formulation and

interpretation," IEEE Trans. Antennas Propag. **35**, 80–86 (1987).

3. E. Heyman and L. B. Felsen, "Weakly dispersive spectraltheory of transients (STT), part II: evaluation of the spectral integral," IEEE Trans. Antennas Propag. **35**, 574–580 (1987).

4. T. B. Hansen and A. D. Yaghjian, "Planar near-field scanning in the time-domain. Part I: fomulation," IEEE Trans. Antennas Propag. **42**, 1280–1291 (1994).

5. T. Melamed, "Phase-space beam summation: a local spectrum analysis for time-dependent radiation," J. Electromagn. Waves Appl. **11**, 739–773 (1997).

6. E. Heyman and T. Melamed, "Space-time representation of ultra windband signals," in *Advances in Imaging and Electron Physics* (Academic, San Diego, Calif., 1998), Vol. 103, pp. 3–63.

7. E. Heyman, "Pulsed beam propagation in an inhomogeneous medium," IEEE Trans. Antennas Propag. **42**, 311–319 (1994).